Pergamon

Journal of Structural Geology, Vol. 17, No. 12, pp. 1689 to 1706, 1995

0191-8141/95 $9.50+0.00

0191-8141(95)00062-3

Granite emplacement during contemporary shortening and normal faulting: structural and magnetic study of the Veiga Massif (NW Spain)

T. ROMAN-BERDIEL,*† E. L. PUEYO-MORER*‡ and A. M. CASAS-SAINZ*

*Departamento de Geología, Facultad de Ciencias, Universidad de Zaragoza, 50009 Zaragoza, Spain
†Géosciences Rennes, Université de Rennes, 1. 35042 Rennes Cedex, France
‡Institut de Ciències de la Terra 'Jaume Almera', C.S.I.C., 08028 Barcelona, Spain

(*Received* 7 *September* 1994; *accepted in revised form* 16 *May* 1995)

Abstract—The Veiga Massif belongs to the calc-alkaline series of Hercynian granitic rocks of the Ibero-Armorican arc. The Veiga granodiorite intruded during the Upper Carboniferous into the core of the WNW–ESE N-verging 'Ollo de Sapo' antiform, formed by Precambrian and Palaeozoic metasediments. Internal fabrics show that magma intrusion was contemporary with shortening. Measurements of feldspars orientations and anisotropy of magnetic susceptibility (AMS) throughout the granite are consistent and indicate a foliation striking WNW–ESE (parallel-to-folding), with a constant dip of 75–85°N. The zonation of bulk low-field susceptibility is related to mineral content and indicates a more basic composition at the southern and western borders. The difference in elevation between outcrops (more than 600 m) allows us to infer the three-dimensional attitude of granite fabrics throughout the Massif. Syn-magmatic fabric folds are preserved in the inner part of the igneous body. The highest degree of magnetic anisotropy is observed in areas located near the bottom and top of the intrusion. At the scale of the Massif, foliation is convergent toward the bottom of the intrusion, along a line located at its northern border, where the magma source is interpreted to be located. In the western border of the Massif, the presence of *C* and *S* structures indicates that magma cooling was coeval with movement of the Chandoiro fault, a N–S striking normal fault with a N290E hanging wall displacement direction. These results indicate that emplacement of the Veiga granite is coeval with NNE–SSW shortening and with an WNW–ESE extension direction, parallel to the trend of the late folds.

INTRODUCTION

Mechanisms of granitoid intrusion have been extensively discussed in the geological literature (Pitcher 1979, Bateman 1984, Castro 1987, Wickham 1987, Miller *et al.* 1988, Hutton 1988, Kukowski & Neugebauer 1990, Paterson & Fowler 1993). Ascent of magma can occur in different tectonic regimes. Granites intruded in extensional, thrust and wrench regimes can be found in the Hercynian Massif of Iberia related to different stages in the evolution of the Variscan orogen (Brun & Pons 1981, Courrioux 1983, Courrioux *et al.* 1986, López-Plaza & Gonzalo 1986, Castro 1986, Corretgé *et al.* 1989, Aranguren & Tubía 1992). The difficulties for clearly identifying the mechanism of intrusion lie in the very nature of igneous rocks: the methods commonly used in structural geology are very useful to study the effects of ductile deformation, but magmatic foliation is hard to measure.

Determination of the anisotropy of the magnetic susceptibility (AMS) is demonstrated to be a powerful tool for determining fabrics in igneous rocks (Heller 1973, Hrouda 1982, Parés 1988, Guillet *et al.* 1983). Some attempts have been made to use the intensity of magnetic susceptibility as an indicator to determine petrographic types (Gleizes *et al.* 1993, Leblanc *et al.* 1994).

This paper aims to study the conditions of emplacement of the granodioritic Veiga Massif and the deformation that affects it. The Veiga Massif is an igneous body intruded in the northern part of the Hercynian belt of Spain, between the Central Iberian and the Western Asturian–Leonese zones (Fig. 1). The main objective of this work is to analyse the relationship between fabric orientation in granites, the magnetic fabric and continuous ductile deformation (taking into account the importance of three-dimensional analysis in the study of magmatic bodies). We also attempt to correlate the emplacement and deformation of the Veiga granitoid within the frame of the tectonic evolution of the northern Iberian Variscan belt. The methodology used in this work includes analysis of magnetic properties of igneous rocks and kinematic analysis of ductile planar and linear fabrics.

GEOLOGICAL SETTING

The Iberian Massif is part of the European Hercynian Orogen. It is classically divided into five zones according to stratigraphic, petrologic and structural features (Lotze 1945, Julivert *et al.* 1972) (Fig. 1): Cantabrian, Western Asturian–Leonese, Central–Iberian, Ossa–Morena and South–Portuguese.

The structure of the northern part of the Iberian Hercynian belt is characterized by a westward-facing arc, formed by several stacked thrust units. Several tectonic stages have been distinguished, most of them corresponding to an overall east–west shortening (Bard *et al.* 1973). The first stages formed recumbent folds and east-verging thrusts; deformation continued forming

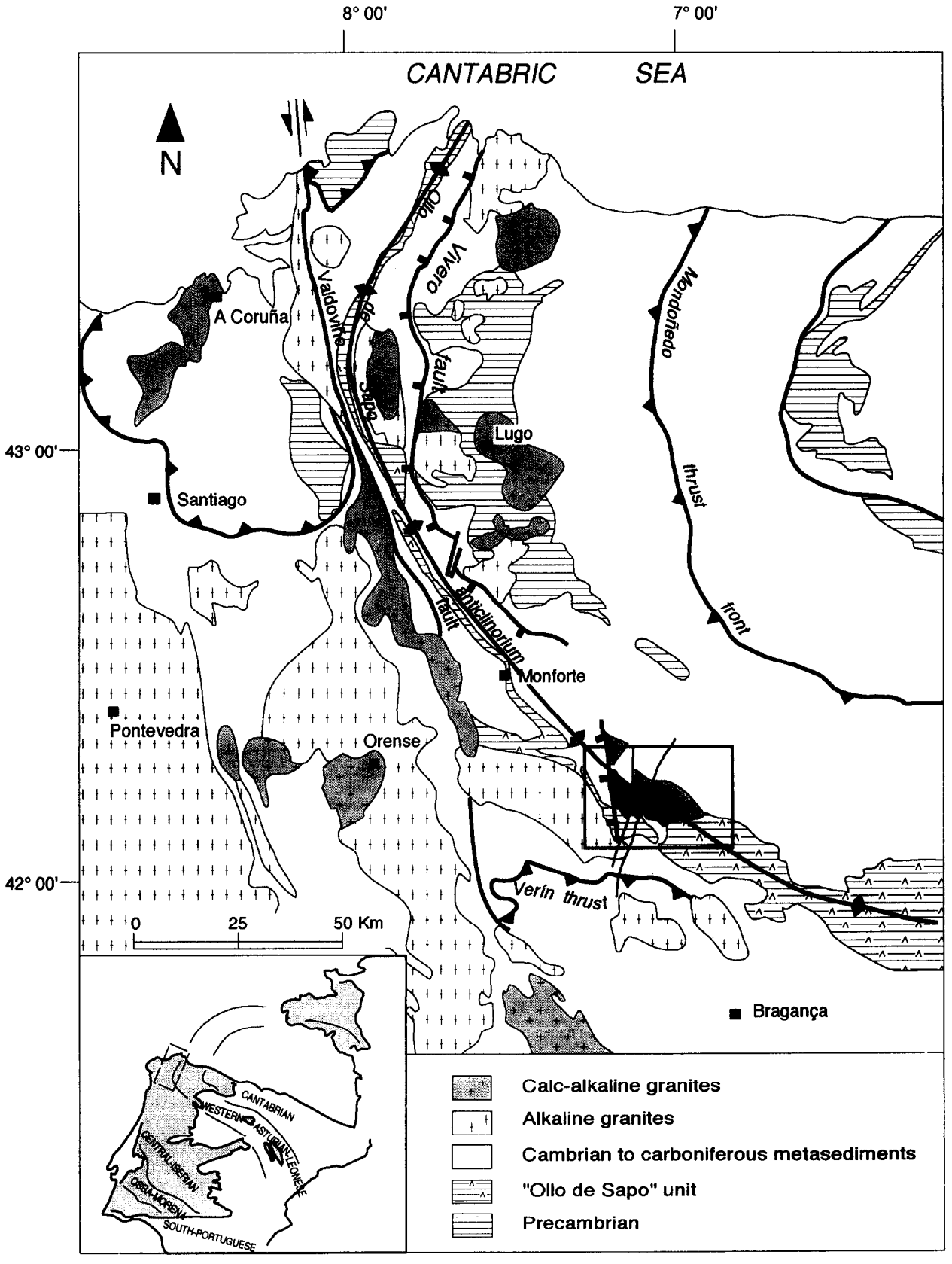

Fig. 1. Geological sketch map of the northern part of the Iberian Hercynian Massif, with the location of the area studied.

vertical folds, both parallel and perpendicular to the trend of the arc. There was a migration of deformation with time, from west (the internal zone of the orogen) to east (external zone). The main extensional structure recognized until now within the northern part of the Iberian Massif is the Vivero fault, with an arcuate shape that follows approximately the trace of the Iberian arc. It indicates an east–west extension, probably due to the collapse of the orogenic wedge after thrusting (Martínez-Catalán 1985, Aranguren & Tubía 1992). The

last stages correspond to Late Variscan brittle deformation (Arthaud & Matte 1977). Regional metamorphism is multi-facial, final stages occurring at low pressure, with localized thermal anomalies due to emplacement of granitoids.

Granitoids are more abundant in the internal (western and southern) zones of the Iberian Hercynian Massif. They have been classically divided into two series, from the chemical and petrologic points of view (Capdevila & Floor 1970): calc-alkaline (I granitoids) and alkaline (S granitoids). At the beginning of the Hercynian orogeny, small bodies and veins of two-mica and calc-alkaline granites appeared. Intrusion of granites began during the thrust stage. Two-mica granites are also associated to after-thrusting NNE–SSW right-lateral and N–S left-lateral shear bands (Iglesias & Choukroune 1980, Aranguren & Tubía 1994). During and after the late folding stage syn- to post-kinematic calc-alkaline bodies were intruded (López-Plaza & Martínez-Catalán 1987).

The Veiga Massif in its geological environment

The Veiga Massif is an intrusive, E–W trending elongated body with dimensions of 20 × 8 km (Fig. 2). Its composition is basically a granodiorite, with local variations to syeno-granite and monzo-granite. Its mineralogical composition mainly consists of quartz, oligoclase, K-feldspar (perthitic orthoclase and microcline) and biotite. Apatite, zircon, muscovite, tourmaline and epidote (allanite) appear as accessory minerals. The texture is porphyritic, with euhedral K-feldspar phenocrysts, that range in size from 2 to 5 cm, within a medium- to coarse-grained matrix. Fine-grained xenoliths, with quartz-diorite composition, are very common. Country rock xenoliths are rare and occur at the borders of the intrusion.

The Veiga Massif is bordered by metasediments whose age range from Precambrian to Ordovician (Fig. 2). They can be divided into three units according to recent studies by Martínez-García & Quiroga (1993): (1) The Viana unit, which consists of gneiss, mica-bearing schists and amphibole-bearing quartzites. Their age is attributed to the Early Cambrian (Martínez-García 1971, 1973) and Late Proterozoic (Ferragne 1972); (2) The Ribadelago unit, which consists of glandular gneiss of the 'Ollo de Sapo' formation, attributed to the Lower Cambrian–Ordovician (Martínez-García 1969, 1973), and also to the Late Proterozoic (Bard *et al.* 1972, Ribeiro 1974); (3) The Peña Trevinca unit, consisting mainly of Cambro-Ordovician schists and quartzites. The contacts between these three units are low angle parallel thrusts that give the sequence, from bottom to top, Viana–Ribadelago–Peña Trevinca throughout the studied area (Martínez-García & Quiroga, 1993). To the southwest of the Veiga Massif lies the Manzaneda two-mica granite.

The overall structure of the studied area is dominated by the 'Ollo de Sapo' anticlinorium, the easternmost unit of the Central–Iberian zone, within the Iberian Massif. It is a large structure developed by the superposition of D_3 over D_1, two deformational phases of the Hercynian orogeny. This anticlinorium, strongly modified by subsequent deformation episodes (Matte 1968, Martínez-Catalán *et al.* 1977, Bastida *et al.* 1993), extends from the Cantabrian Sea to the Spanish Central Massif. Its trend changes from N030E to N110E, following the shape of the Iberian arc. In the country rocks of the Veiga Massif the following structural events have been distinguished (Barrera-Morate *et al.* 1989):

(1) D_1 produced cleavage-related folds trending N110–150E (classes 1c to 2 of Ramsay 1967) with axes plunging from 20°NW to 25°SE.

(2) D_2 produced NE-verging thrusts: the most important are the Verín thrust, with an estimated 150 km horizontal displacement, and the Pradocabalos thrust, associated with crenulation cleavage and nearly horizontal micro-folds (Ribeiro 1970, 1974, Marcos 1971, 1973, Martínez-Catalán 1985, Bastida *et al.* 1986, Farias 1990).

(3) The western part of the Veiga Massif is cut by the N–S striking 55–70°W dipping Chandoiro normal fault (Fig. 2), with a mapped length of about 30 km. It formed after the second deformation phase, and it is possibly contemporary with the subsequent D_3.

(4) D_3 produced gentle folding of the former structures. Main folds trend NW–SE and verge NE (Parga-Pondal 1963, Gonzalez-Lodeiro & Iglesias 1977). These structures are associated with crenulation cleavage and stretching lineation parallel to fold axes.

The major structure in our study area is therefore a D_1 anticlinorium refolded by D_3. Related metamorphism began during the first stage and reached a maximum between the D_2 and D_3 phases. Its intensity increases toward the southwest. Retrograde metamorphism, hydrothermal metamorphism and cataclasis affected the rocks located near the Chandoiro normal fault.

The Veiga Massif developed a metamorphic aureole in the country rocks. Contacts are parallel to the regional cleavage trajectories in the northern and southern border of the Massif but cut across them in the eastern and western parts. Finally, the Veiga Massif is cross-cut and displaced by two Late Variscan faults that show an apparent left-lateral strike-slip movement.

RESEARCH METHOD

Ductile deformation

The analysis of ductile deformation in the granite is based upon both the magmatic foliation and *C–S* structures. These structures allow to determine the geodynamic context during the emplacement of magmatic bodies (Berthé *et al.* 1979, Iglesias & Choukroune 1980, Gapais & Barbarin 1986, Gapais & Cobbold 1987, Lagarde 1987, LeCorre & Saquaque 1987, Vauchez 1987). The *C–S* structures are present in the western border of the Veiga granite, near the Chandoiro fault. Their systematic analysis was made to determine the width of the shear zone and the change of intensity of deformation from west to east. Moreover, kinematic data and tem-

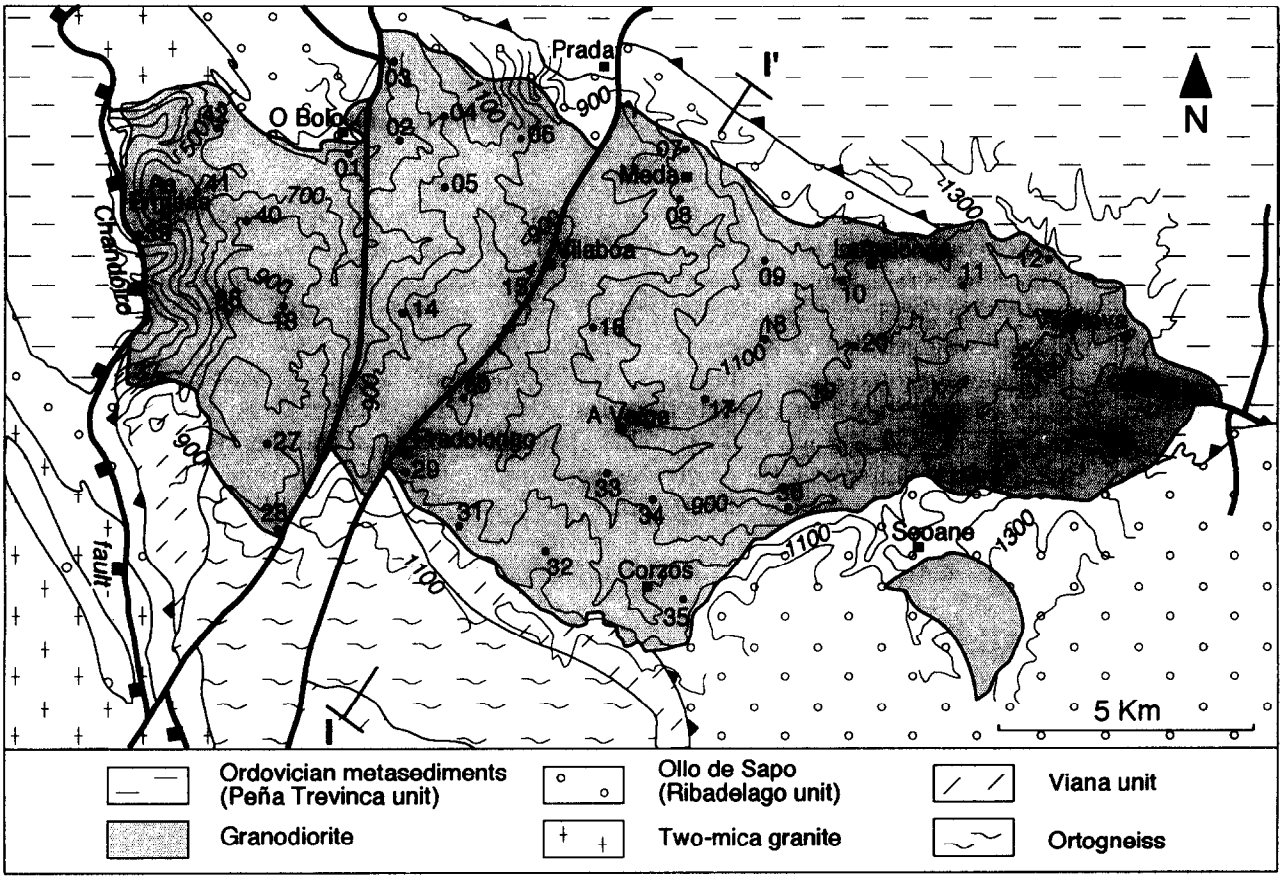

a

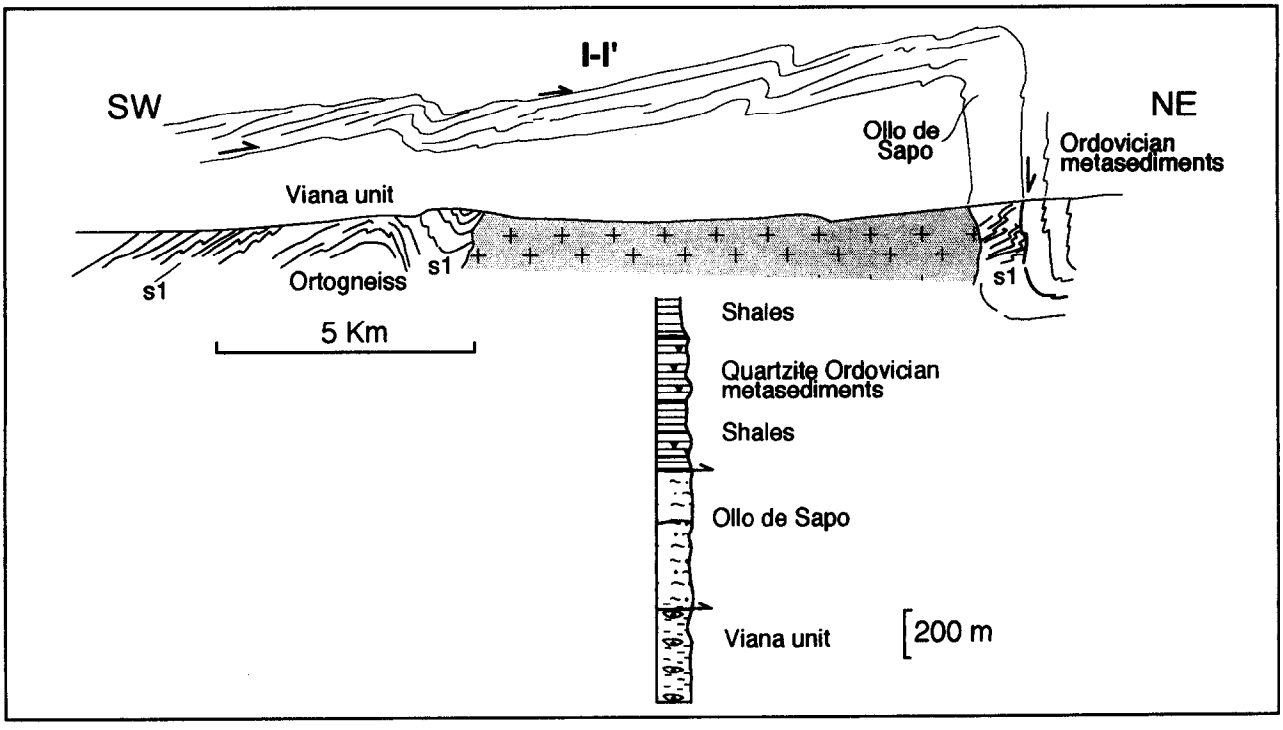

b

Fig. 2. (a) Geological sketch map of the Veiga Massif, simplified from Iglesias & Varea (1982), with location of measurement sites. Contours show present-day topography (numbers indicate elevation above sea level). (b) Cross-section of the Veiga Massif, modified from Iglesias & Varea (1982).

perature estimates were obtained from the analysis of quartz *c*-axis fabrics of several samples. In order to determine the orientation of magmatic foliations and lineations, systematic measurement of (010) planes and *c*-axes of feldspar phenocrysts was carried out in 40 sites; these sites are homogeneously distributed throughout the outcropping surface of the Veiga Massif (see Fig. 2), with a total of nearly 1000 crystals measured. Data statistics were made of their distribution in sterographic projection, considering both the orientation of absolute maxima and the distribution of relative maxima.

AMS analysis

Anisotropy of magnetic susceptibility is a useful tool for determining the conditions of emplacement of granitoids by interpretation of the internal structure, because of the suitable treatment of tensorial data, i.e. principal axes, orientations and moduli, and the relationship between them.

Forty-two sites in an area of about 154 km^2 were analyzed (Fig. 2). They are homogeneously distributed throughout the Veiga granodiorite. The sites were core-drilled and the cores were oriented in the field. In each site we obtained two–seven cores (see Table 1), with an average of five cores. These five cores are distributed homogeneously, considering both the sampled rock surface (spatial distribution) and the orientation of their axes. This procedure of sampling allows testing of the reliability of AMS measurements in moduli (magnetic susceptibility averages), orientations of the tensor principal axes (K_1, K_2, K_3) and scalar ratios (see below). The results were obtained from an average of six specimens per site.

Fifteen measurements were taken and referred to a diagonal matrix. Measurements were made with a KLY-2 susceptibility meter, using a bridge at low magnetic field. The relationship between tensors axes, normalized by means of Jelinek's method (Jelinek 1977, see Table 1), was studied using the corrected anisotropy degree P' and the shape parameter, T, defined as (Jelinek 1981):

$$P' = \exp \sqrt[2]{\{[(\mu_1-\mu_m)^2 + (\mu_2-\mu_m)^2 + (\mu_3-\mu_m)^2]\}} \quad (1)$$

$$T = (2\mu_2-\mu_1-\mu_3)/(\mu_1-\mu_3), \quad (2)$$

where $\mu_1 = \ln K_1$, $\mu_2 = \ln K_2$, $\mu_3 = \ln K_3$ and $\mu_m = \sqrt[3]{(\mu_1 \cdot \mu_2 \cdot \mu_3)}$.

RESULTS

Fabrics within the pluton

From the structural point of view, the Veiga Massif is homogeneous at the outcrop scale except on its western border. Feldspar phenocrysts are euhedral and show no evidence of plastic deformation. Quartz crystals are coarse-grained with moderate internal deformation, as represented by undulose extinction.

The orientation of nearly one thousand K-feldspar megacrysts, distributed over 40 sites were measured, with an average of 30 crystals per site. At most sites, the orientation of (010) planes was measured, but because of poor outcrop conditions, the orientation of *c* axes of feldspar crystals could not be measured at every site (Fig. 3). At sites with a high number of measurements, two types of distribution can be seen: (1) a planar type, where the orientation of *c*-axes of feldspars is distributed according to a great circle that coincides with the maximum of (010) planes orientations; and (2) a linear type, where maxima of (010) planes lie along a great circle whose pole defines the lineation. Planar fabrics show a WNW–ESE strike (Fig. 4), steeply dipping to the north. This general attitude of (010) planes is clear in the northern and southern borders of the Massif (Fig. 4). On the contrary, the central part of the Massif shows a higher dispersion of foliation, with several N–S striking relative maxima and some subhorizontal measurements.

The western border of the Veiga Massif is affected by the Chandoiro normal fault. The *C–S* structures indicating normal shear with top-to-the-west movement can be seen in a 3 km wide band inside the pluton. The *C* planes, where biotite crystals concentrate, show a regular spacing of about 3 cm, and a strong 120°E-trending stretching lineation can be seen on them. The maximum density of orientations of the stretching lineation on *C* planes is 292, 57 (Fig. 4). Shear planes strike NNE–SSW and dip 44–85° to the west. A less conspicuous conjugate set of *C* planes, dipping 27–45°W with reverse (top-to-the-east) movement has also been observed. Between *C* planes, rotated euhedral feldspar phenocrysts have been observed in outcrop and in thin section (Figs. 5a & c). The foliation shows a sigmoidal shape consistent with the shear sense, with decreasing grain size towards the shear bands. A change in the quartz fabric over shear planes is revealed by the gradual strengthening of the quartz fabric toward the shear bands (Fig. 5b), and by the development of a shape foliation defined by elongated recrystallized grains of quartz within the *C* domains (Fig. 5b). Biotite crystals are deformed by kink bands (Fig. 5d). Microcline crystals show late reactions forming myrmekite textures (Fig. 5e) (Simpson 1985). The fact that biotite crystals are concentrated on *C* planes and are also deformed by kink bands indicate that deformation was coeval with the cooling process of the Massif.

The crystallographic orientation of *c*-axes of quartz grains was measured in four thin sections from *XZ* surfaces with a Universal Stage (Fig. 6). Outside the western shear zone (Figs. 6a & b), quartz has a composite crystallographic preferred orientation of *c*-axes: two maxima are close to the maximum stretching direction *X* whereas other relative maxima are located close to *Y*. This pattern suggests activation of prismatic slip on both *a*- and *c*-directions. Alternatively, it could be interpreted as the result of a selective grain boundary migration parallel to the *c*-axis at high-temperature conditions (Gapais & Barbarin 1986, Tommasi *et al.* 1994). In the western shear zone, the crystallographic

Table 1. The AMS results. *S*: site number, *Nc*: number of cores drilled in each site, *n/N*: number of specimens considered/number of specimens analysed at each site (some specimens, *N–n* in number, are not considered due to its very high residual error; Jelinek 1977), *ε*: standard error, P′: corrected anisotropy degree (Jelinek 1981); *T*: shape parameter (Jelinek 1981); *Km*: arithmetic mean of bulk susceptibility for the site (in 10^{-6} SI); K_1, K_2 and K_3: mean (trend/plunge) of AMS axis orientations considering a unimodal distribution (Fisher 1953), α_{95}: opening angle for the confidence cone with the 95% probability; *K*: accuracy parameter, E_3, $|E_3|$: trend/plunge and modulus of eigenvectors of K_1 and K_2 distributions.

	S	Nc	n/N	K1	α95	k	E3	|E3|	K2	α95	k	E3	|E3|	K3	α95	k	P′	ε	T	ε	Km	ε
NORTHERN	1	6	6 / 6	287/00	10	35	--------	------	018/48	14	19	287/02	0.0323	196/43	13	20	1,042	0,004	0,241	0,092	106	13
	2	7	4 / 6	125/14	12	33	347/72	0.0028	018/53	10	51	--------	------	225/36	13	30	1,037	0,002	0,254	0,133	169	34
	3	4	6 / 6	112/24	9	40	--------	------	321/64	16	13	084/15	0.0173	210/09	15	17	1,033	0,002	0,054	0,095	166	11
	4	4	6 / 6	093/33	11	33	203/28	0.0087	313/50	13	21	124/33	0.0030	198/19	9	41	1,041	0,003	0,507	0,077	117	12
	5	6	5 / 6	115/03	6	100	--------	------	021/51	7	92	--------	------	208/38	3	380	1,04	0,006	0,254	0,132	103	21
	6	4	6 / 7	115/32	8	47	--------	------	315/57	16	14	132/34	0.0089	208/10	15	15	1,035	0,002	0,462	0,091	93	6
	7	3	3 / 3	132/10	12	51	236/54	0.0069	031/62	28	10	137/8	0.0191	226/28	27	10	1,015	0,003	0,144	0,44	76	10
	8	4	4 / 5	114/21	17	18	220/35	0.0275	305/68	23	11	142/20	0.0296	203/06	22	11	1,029	0,003	-0,011	0,228	122	5
	9	5	4 / 6	094/14	14	28	307/74	0.0118	216/68	17	18	080/17	0.0281	359/20	19	15	1,028	0,003	0,051	0,21	103	7
	10	3	4 / 5	099/07	14	25	004/36	0.0096	325/78	14	28	154/12	0.0126	188/07	13	30	1,022	0,003	-0,317	0,084	97	9
	11	5	6 / 7	084/38	17	20	205/33	0.0384	304/40	16	13	072/36	0.0298	194/22	17	12	1,043	0,005	0,456	0,08	77	13
	12	5	6 / 6	070/32	11	31	238/57	0.0018	339/02	11	29	247/45	0.0045	246/57	4	210	1,039	0,003	0,081	0,173	116	10
CENTRAL	13	7	5 / 6	304/03	13	24	034/40	0.0284	211/32	19	12	115/07	0.0350	046/58	15	18	1,026	0,003	-0,026	0,1	124	12
	14	7	6 / 6	351/07	22	8	239/73	0.0286	087/37	24	7	238/49	0.0553	247/55	14	18	1,054	0,009	0,426	0,112	16	2
	15	5	7 / 7	134/16	12	20	301/74	0.0132	022/55	10	31	--------	------	235/32	11	25	1,034	0,005	0,175	0,085	139	33
	16	4	6 / 8	307/08	8	54	--------	------	072/68	20	9	314/10	0.0111	213/18	22	8	1,051	0,005	0,142	0,139	49	2
	17	4	6 / 6	017/16	16	14	241/68	0.0105	111/17	17	12	230/58	0.0297	242/66	9	46	1,038	0,001	0,357	0,101	130	13
	18	5	6 / 6	039/13	17	12	277/68	0.0113	138/32	18	11	256/37	0.0247	284/55	14	24	1,037	0,004	0,337	0,081	95	14
	19	6	7 / 9	091/56	46	2	226/27	0.0704	003/64	55	1	216/25	0.0617	221/25	15	14	1,042	0,003	0,541	0,054	82	10
	20	2	2 / 2	023/14	8	43	--------	------	262/64	1	2193	--------	------	119/22	8	44	1,026	0,004	-0,196	0,004	128	7
	21	4	4 / 5	073/55	80	2	210/27	0.0040	069/53	72	2	219/32	0.0216	214/30	14	45	1,041	0,004	0,272	0,12	109	19
	22	6	6 / 6	023/08	17	13	134/68	0.0331	300/04	22	8	207/37	0.0995	197/80	18	12	1,037	0,004	0,012	0,201	82	3
	23	4	3 / 4	132/76	16	27	285/12	0.0091	280/14	29	9	090/76	0.0053	012/09	33	7	1,027	0,004	0,411	0,189	110	11
	24	6	7 / 9	118/20	22	7	216/23	0.1044	246/71	22	7	038/17	0.1123	025/12	21	8	1,031	0,002	0,081	0,13	97	7
	25	5	6 / 6	133/27	16	14	232/16	0.0214	010/46	16	14	255/22	0.0329	243/29	10	32	1,038	0,002	0,075	0,192	54	4
	26	4	4 / 4	129/01	19	11	009/88	0.0036	219/10	19	10	356/77	0.0160	024/81	6	80	1,065	0,003	0,458	0,031	130	7
SOUTHERN	27	5	6 / 7	315/31	16	13	198/33	0.0157	046/36	20	9	223/54	0.0698	191/46	14	19	1,022	0,002	-0,036	0,118	123	9
	28	5	5 / 5	313/21	12	30	184/59	0.0050	103/67	11	35	335/15	0.0166	218/12	13	25	1,042	0,004	0,291	0,076	187	11
	29	5	4 / 5	116/51	72	2	231/15	0.0231	008/64	76	2	217/27	0.0393	226/20	23	17	1,03	0,006	0,619	0,08	280	17
	30	6	6 / 6	119/42	47	3	226/19	0.0058	353/65	46	3	224/15	0.0169	225/16	7	78	1,029	0,004	0,606	0,063	141	4
	31	4	6 / 6	336/30	18	11	231/24	0.0194	115/54	19	11	243/24	0.0233	235/21	9	42	1,032	0,003	0,661	0,058	153	14
	32	4	4 / 5	357/61	36	5	223/21	0.0064	118/18	36	5	212/09	0.0079	217/18	9	64	1,04	0,003	0,465	0,105	176	13
	33	4	4 / 5	324/41	24	10	211/25	0.0032	102/41	24	10	207/17	0.0041	212/22	8	146	1,042	0,002	0,484	0,117	180	21
	34	5	6 / 6	299/16	16	15	207/04	0.0271	062/64	16	15	196/20	0.0329	201/19	12	28	1,033	0,004	0,618	0,088	158	6
	35	3	5 / 5	337/47	47	3	200/34	0.0098	086/17	46	3	190/42	0.0063	194/38	10	66	1,032	0,001	0,534	0,144	173	21
	36	4	4 / 4	014/84	24	10	207/06	0.0287	106/01	22	11	195/02	0.0059	197/05	11	46	1,039	0,002	0,616	0,142	136	13
WEST	37	3	3 / 3	286/20	6	216	--------	------	034/41	7	137	--------	------	176/42	5	300	1,065	0,001	0,147	0,08	113	11
	38	5	6 / 6	302/20	7	77	--------	------	208/10	9	38	--------	------	092/67	8	49	1,063	0,003	-0,309	0,045	120	14
	39	5	3 / 4	287/18	6	182	--------	------	196/03	3	505	--------	------	097/72	5	264	1,071	0,004	-0,134	0,036	104	5
	40	6	6 / 6	289/12	9	43	--------	------	022/08	13	22	115/24	0.0140	138/74	11	29	1,04	0,004	-0,023	0,081	158	22
	41	3	3 / 3	298/19	6	193	--------	------	203/15	6	185	--------	------	076/65	4	433	1,051	0,003	-0,046	0,056	143	18
	42	4	4 / 6	119/01	17	18	210/43	0.0113	028/38	19	14	192/57	0.0000	206/51	13	32	1,042	0,003	0,017	0,147	99	8

preferred orientation of quartz suggests activation of basal slip: two maxima are close to *Z* (Figs. 6c & d). The orientation of other sub-maxima indicates prismatic slip in the *a*-direction (Lister & Williams 1979, Bouchez & Pêcher 1981, Gapais & White 1982, Gapais & Barbarin 1986). This change in the main slip systems between the western shear zone and the rest of the Massif indicates that temperature decreases from east to west.

AMS results

Because of its low susceptibility (*Km* is comprised between 90×10^{-6} and 170×10^{-6} SI) (Table 1), the Veiga granitoid can be considered as a 'non-magnetic' granite according to the classification of Ellwood & Wenner (1981), and as a rock with dominant paramagnetic susceptibility according to Rochette (1987). Biotite

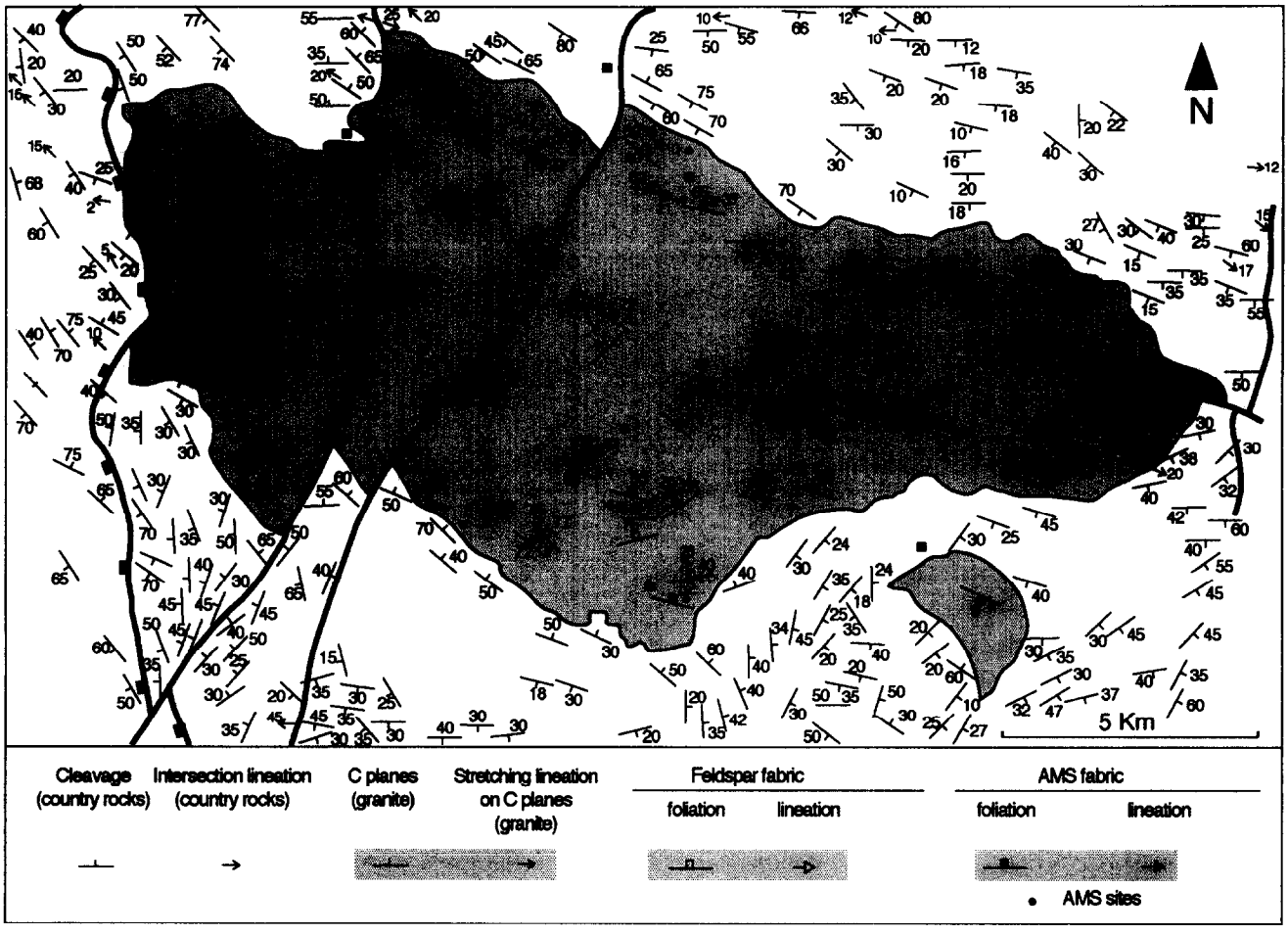

Fig. 3. Foliations measured from feldspar phenocrysts (average obtained in every site), *C–S* structures and magnetic anisotropy (AMS) in the Veiga Massif, and cleavage measured in country rocks.

(and, to a lesser extent, ilmenite) constitutes the main paramagnetic contribution. Therefore, the map showing the spatial variations of *Km* (Fig. 7) mainly reflects the biotite content. The *Km* zonation (Fig. 7) shows maximum values at the southern border, gradually decreasing toward the central part. This distribution agrees with observations of thin-sections along N–S transects, which show an increase in biotite content from north to south. Near the northern border, *Km* values increase again but contours do not completely outline a concentric pattern.

The magnetic planar fabrics show a high degree of consistency with the foliation planes determined from the orientation of feldspar megacrysts: the orientation of K_3 axes coincides with poles of (010)-feldspar planes (see Figs. 3 and 4a). Where the magnetic lineation can be defined (in triaxial or prolate ellipsoids), it is subhorizontal with an E–W trend at the northern border and a variable trend in the central sector and at the southern border. This lineation shows a high degree of consistency with the lineation determined from *c*-axes of feldspar megacrysts (see Fig. 3). At the western border, near the shear band linked with the Chandoiro fault, K_1–K_2 planes are oblique to *C* planes and parallel to the foliation determined by the orientation of feldspar megacrysts (see Fig. 3 and Table 1). The K_1 axes (see Fig. 4b) are parallel to the projection of the stretching lineation (measured on *C* planes) on the foliation planes (see Fig. 4b).

The degree of anisotropy of the magnetic ellipsoid *P'* (Table 1) is maximum in the western part of the Massif and related to ductile deformation associated with movement of the Chandoiro fault (Fig. 8a). In the rest of the Massif, relative maxima of *P'* appear in two domains: (1) two central areas within the Massif, that approach the bottom of the N–S thalwegs (site 16, Fig. 8a); and (2) the isolated Seoane outcrop at the highest topographic level in the Massif. From these features we infer higher strains at pluton boundaries (floor and roof), especially in the vicinity of the Chandoiro fault.

The shapes of the magnetic ellipsoids (given by *T*, Table 1) is distributed as follows: the southern border of the Massif shows mainly oblate shapes, whereas in the northern part triaxial or prolate shapes dominate (Figs. 8b and 9). In the shear zone of the western boundary, magnetic ellipsoids are triaxial to prolate. The shape of the magnetic ellipsoids can be related to the distribution of the orientation of feldspar planes at different sites (see Fig. 4): at the southern border of the Veiga Massif poles to (010)-feldspar planes tend to be concentrated in one maximum, whereas at the northern border, poles

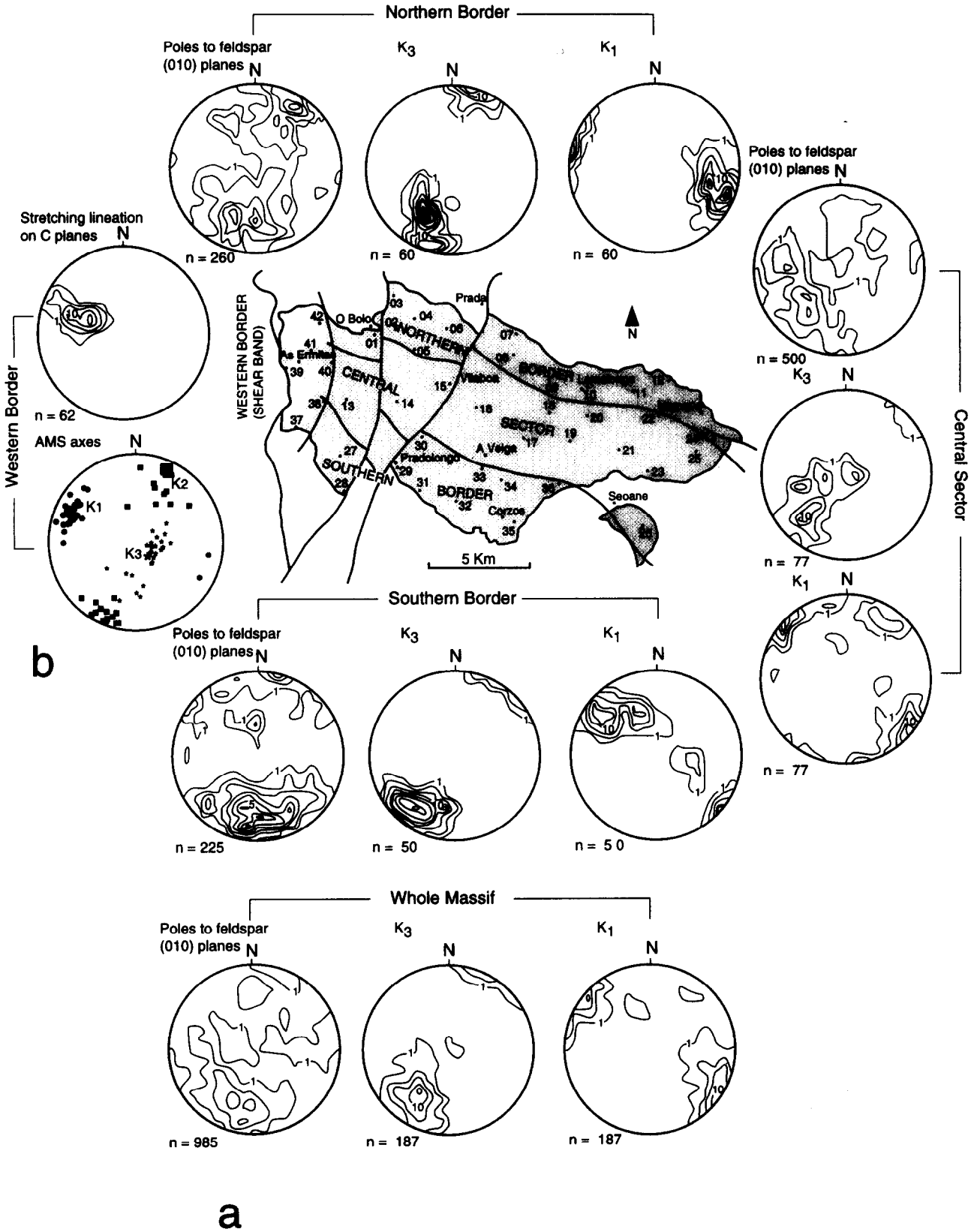

Fig. 4. (a) Density diagrams (Schmidt net, lower hemisphere) of feldspar orientations and AMS axes in the three zones distinguished within the Veiga Massif, and for the whole Massif. Contour intervals: 0.8% for feldspars and 3.0% for AMS data. (b) Density diagram of the stretching lineation in the western part of the Veiga Massif (contour intervals: 3.0%) and stereoplot of AMS axes obtained for each specimen. For the three populations of axes, the Fisher distribution vector has been calculated.

are distributed in great circles perpendicular to the *c*-axes of feldspars. Furthermore, areas where oblate magnetic ellipsoids are observed coincide with areas where no clear preferable orientation of *c*-axes of feldspar are observed in the field.

Comparison of results. Three-dimensional considerations

In the absence of gravity data, structural observations from outcrop at different elevation can help to obtain

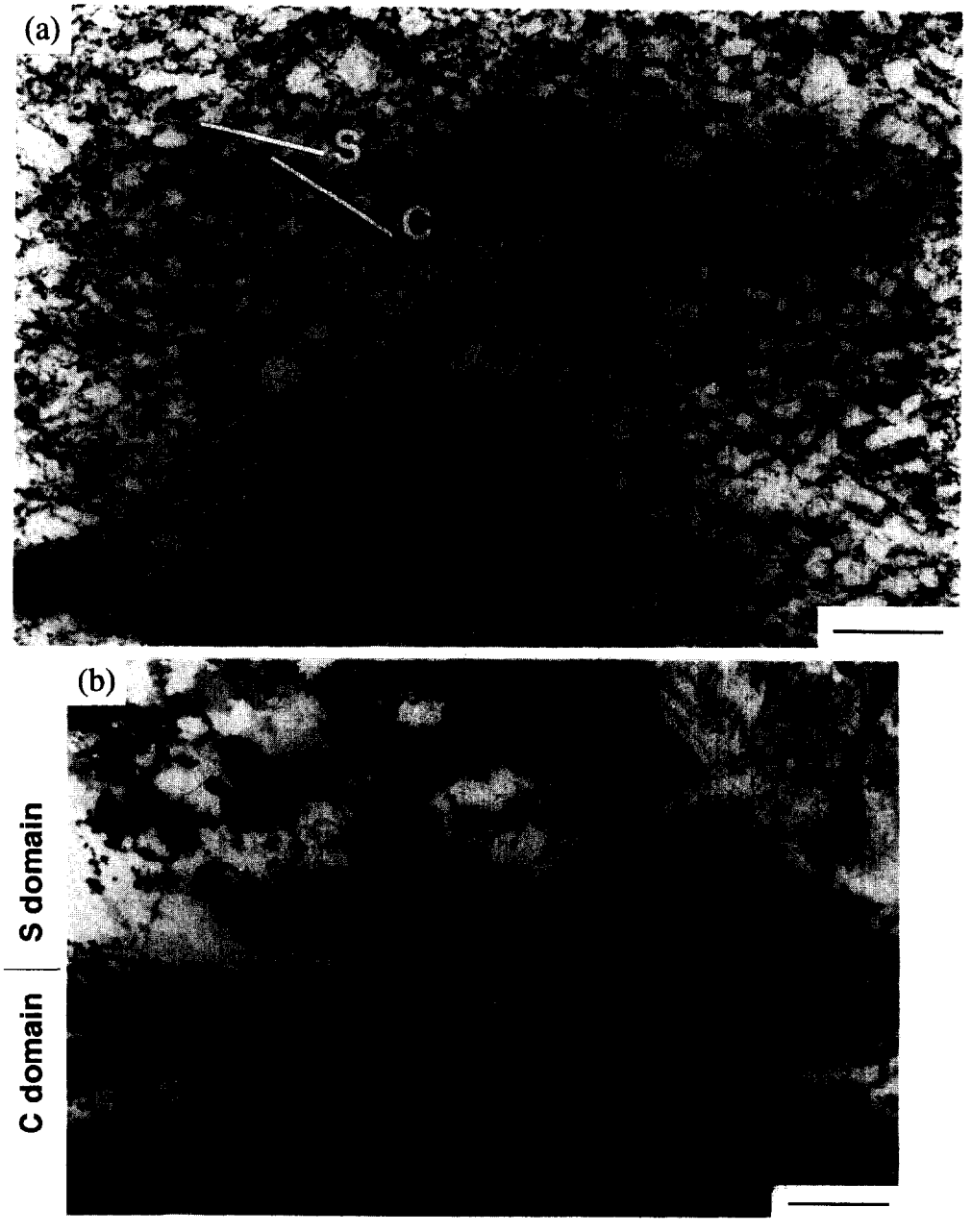

Fig. 5. (a) Field aspect of *C–S* structures in the western part of the Massif. Shear sense is top-to-the right. Scale bar is 5 cm; (b), (c) and (d) are different aspects of a thin section showing mineral strain in this outcrop. Arrows indicate shear sense. (b) Quartz aggregate sheared at the edge of a discrete shear-zone. Scale bar is 1 mm. (c) Rotated euhedral feldspars between *C* planes. Scale bar is 1 mm. (d) Biotite crystal deformed by kink bands. Scale bar is 0.2 mm. (e) Myrmekite intergrowths (M) in the eastern part of the western border, (F) feldspar, (B) biotite, (Q) quartz.

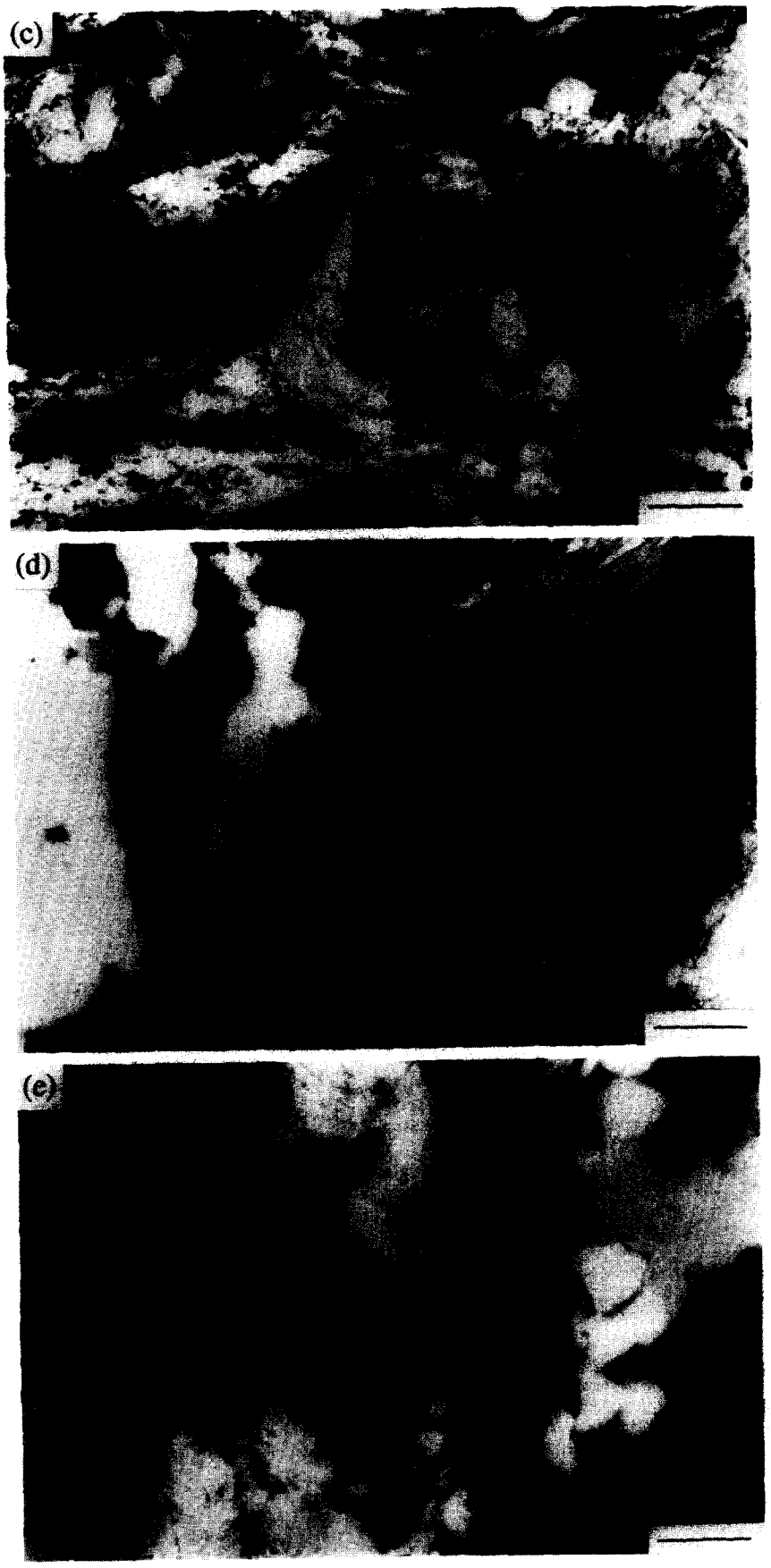

Fig. 5. (c–e).

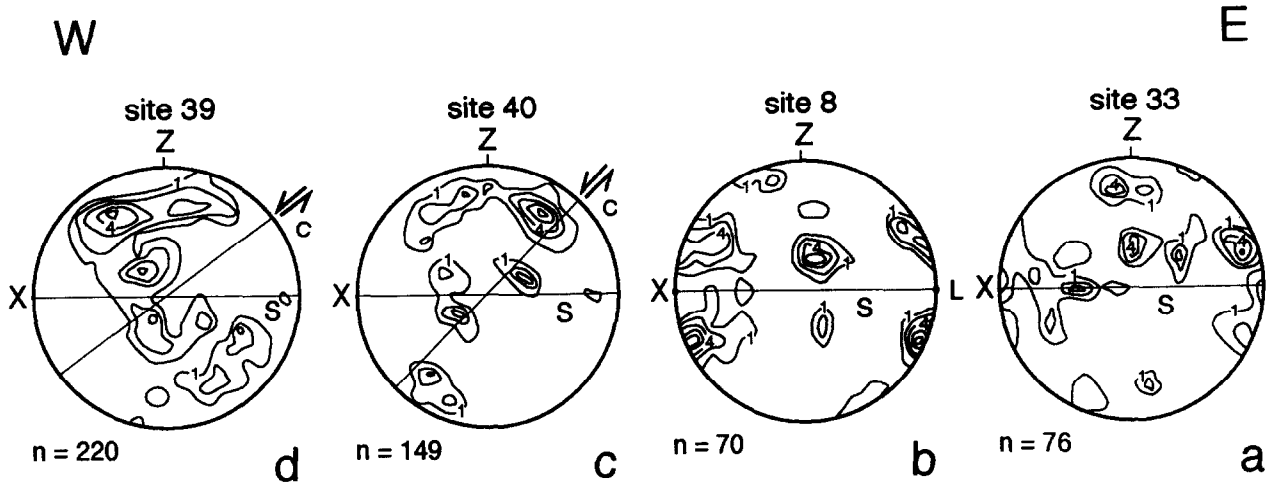

Fig. 6. Quartz *c*-axis fabrics obtained from thin sections measurements at four sites in the Viana granodiorite; (a) and (b) are situated outside the western shear zone, (c) and (d) are situated in the western shear zone; *S* (foliation) and *L* (lineation) are determined from thin section observations. Equal-area, lower-hemisphere; contour intervals are 1.5% in (a), (b) and (c), and 1% in (d).

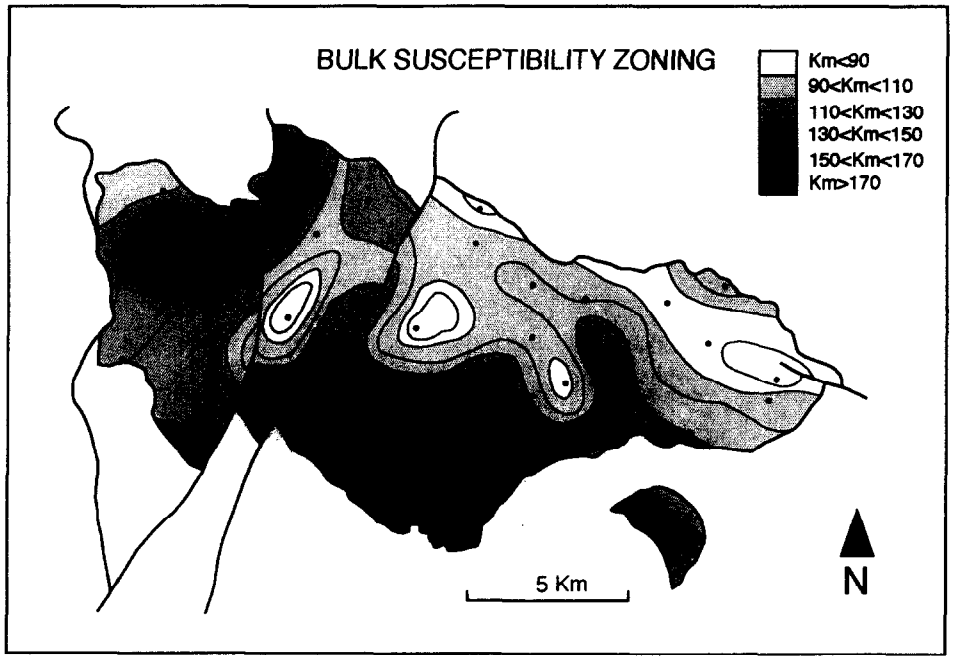

Fig. 7. Bulk susceptibility (*Km*) map ($\times 10^{-6}$ SI) of the Veiga granodiorite.

information on the three-dimensional geometry of a granitic body. From structural and magnetic data, a map of the interpreted trajectories of planes of magmatic foliations and *C*-planes has been drawn (Fig. 10a). Except on its western border, the Veiga Massif is homogeneous at the outcrop scale, with a planar fabric striking WNW–ESE, steeply dipping to the north (Fig. 10a). This foliation is parallel to the principal regional structure. Some irregularities are observed in the central part of the Massif (Fig. 10a), probably related to D_3 folding. At the western border trajectories of *C*-planes striking N–S cut across foliations of the country rock and the granite. The elevation differences between the studied sites (more than 600 m), together with the near-horizontal lineation and the relatively constant strike of the foliation (WNW–ESE) (Fig. 10a), allow projection of our data onto a plane perpendicular to the average strike of the fabric (method described by Roberts 1982). We have projected the dip of foliation planes and the degree of anisotropy of the magnetic ellipsoid *P'* on that plane (Fig. 10b). Note that this projection is not a real cross-section. Data of the western part of the Massif were excluded from this projection, since they show a completely different attitude and are linked to the movement of the Chandoiro fault. From this projection (Fig. 10b) a convergence of foliation toward the lower part of the granite along the northern border can be recognised. Irregularities in foliation orientation concentrate in the central part of the Massif. Here, foliation planes form asymmetric folds: anticlines with strongly dipping north-

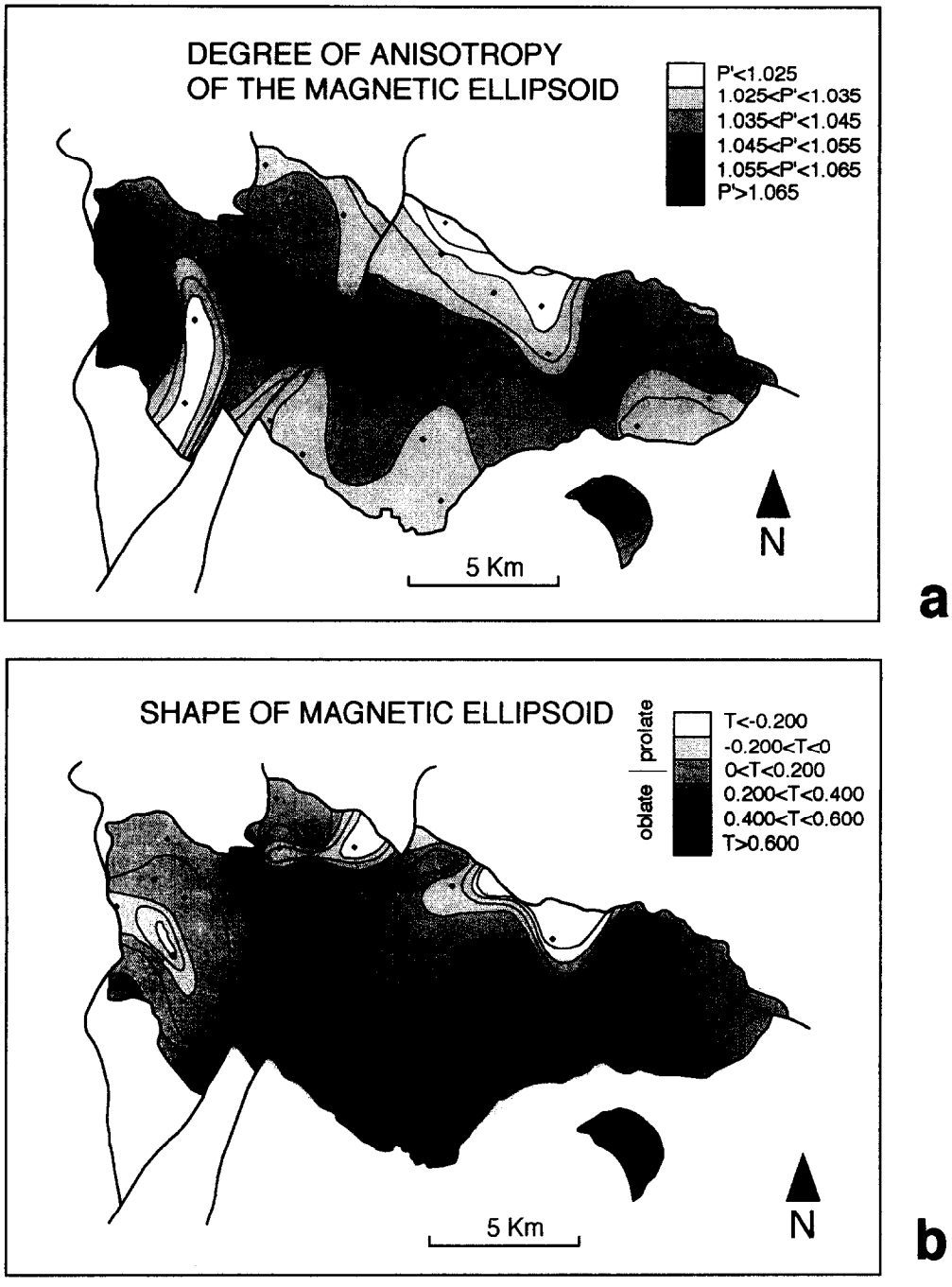

Fig. 8. (a) Map of the anisotropy index P' of the magnetic ellipsoid. (b) Map of the shape parameter T of the magnetic ellipsoids.

ern limbs and gently dipping southern limbs, that could be contemporary with comparable folds found in the country rock. Nevertheless, these irregularities could also correspond to root zones at deeper levels.

The convergence of foliation planes toward the northern lower part of the intrusion suggests the existence of a magmatic source along this northern border. This hypothesis may explain the apparent opposite vergence between the magmatic foliation which is consistently dipping northward, with a steepest dip in the northern sector, and the northward-verging asymmetric anticline within which the Veiga granodiorite intruded (Fig. 11).

Nearly horizontal magmatic lineations that appear in the northern part of the Massif (Fig. 3) are apparently not consistent with the magmatic source hypothesis, but it must be taken into account that they may result from the kinematics of folding coeval with intrusion. The northern limb of the 'Ollo de Sapo' antiform shows the same orientation as the magmatic foliation. The later Hercynian folding produced crenulation cleavage and a horizontal NW–SE stretching lineation parallel to fold axes. This lineation is indicated both by tension gashes in feldspars, filled with NW–SE trending quartz fibres within the 'Ollo de Sapo' formation, and by recrystallization of micaceous minerals (Iglesias & Varea 1982). In the southern part of the Massif, magnetic ellipsoids show

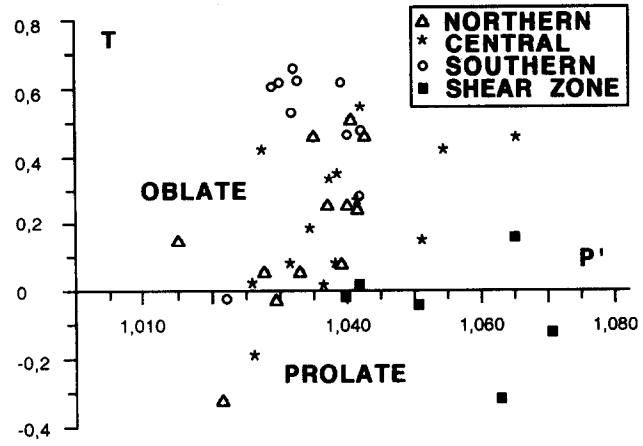

Fig. 9. Representation of P'/T for the different sectors (see Fig. 4) of the Veiga Massif.

a general oblate shape, and the main magmatic foliation dips in the opposite sense as the fold limb. No stretching lineation has been found in this southern limb.

DISCUSSION

Relationship with regional tectonics

The Veiga Massif is interpreted as a WNW–ESE elongated igneous body, with a regular zonation from the southern and western borders (more basic) to the central part and northeastern border (more acid). The fabric anisotropy is maximum near the top and bottom of the intrusion. Foliation directions are parallel to the main regional structure, with irregularities in the central part, probably due to shortening and folding coeval with intrusion. Convergence of foliation at depth toward the northern border of the Massif could indicate a magma source in the northern sector, that interferes with regional NE-verging folding (Fig. 11). Extensional ductile shear with top-to-the-west motion associated with the Chandoiro fault occurred during the late stages of the emplacement of the Veiga granodiorite, under different temperature and strain conditions. In sites located in the easternmost part of the shear zone feldspar phenocrysts strike N120E and dip to the North, whereas *C*-planes indicate WNW extension. In the westernmost part of the shear zone the primary structure of the granitoid is completely obliterated by *C–S* structures, although most feldspar phenocrysts striking N–S maintain their original shape.

No regional widespread cleavage in the country rocks is associated with the WNW–ESE D_3 folding contemporary with the emplacement of the Veiga Massif. Only crenulation cleavage and solid-state lineations developed during this stage. In some areas, the contacts of the Veiga granitoid cut across cleavage trajectories in the country rock. These cleavage planes were formed during D_1 and were folded by D_3 (Fig. 11). Because of the different age of the regional cleavage and the intrusion, the syn-kinematic emplacement of the Veiga Massif is not associated with a systematic pattern of deflection of cleavage trajectories in the country rock, as found in many syn-tectonic granites (Brun & Pons 1981, Brun *et al.* 1990). On the other hand, the development of a primary foliation followed by *C–S* fabrics in the western border of the Veiga Massif is actually typical of syn-kinematic granites, in which temperature decreases during progressive deformation (Gapais & Barbarin 1986).

The Veiga Massif was previously considered as a post-tectonic pluton within the Iberian Massif (López-Plaza & Martínez-Catalán 1987). From the magnetic and structural study presented here it is clear that (1) the intrusion of magma in the Veiga Massif was coeval with NNE–SSW shortening, consistent with the direction defined by the D_3-deformation phase imprinted in the 'Ollo de Sapo' anticlinorium; and (2) cooling of the intrusion is coeval with movement of the N–S Chandoiro normal fault. The intrusion of the Veiga granodiorite happened after the D_2 thrusting stage (here represented by the Verín thrust, that shows a north-northeast transport direction (Farias 1990, see Fig. 1), with deformation controlled by upright or slightly NE vergent D_3 folds. Unfortunately, no absolute dating that could help to accurately locate this deformation stage within the Hercynian orogeny, exists in the Veiga Massif.

Barrera-Morate *et al.* (1989) suggested that the extensional stage responsible for the Chandoiro fault occurred before late D_3 folding, because some N–S normal faults in the Iberian arc are folded. From the analysis of structures in the area studied, it can be seen that the Chandoiro fault is not affected by folding and that the extensional stage postdates late folding. Nevertheless, the two processes (WNW–ENE folding and WNW extension) could coexist for a certain period on the regional scale, giving different chronological relationships between structures in different places. Similar conditions of superposition of strain fields are also described in the recent evolution of other mountain chains (Mancktelow 1992).

Extension contemporary with shortening, usually related with extensional collapse of a thickened crust, is a common scenario in many orogenic belts. Examples are found of extension either parallel or perpendicular to shortening (Ratsbacher *et al.* 1989, Malavieille *et al.* 1990, Tapponnier *et al.* 1981, Malavieille 1992, Mancktelow 1992). Extension perpendicular to shortening is interpreted in terms of switching of deformation axes (when the intermediate axis is near vertical) and there is a decrease in the compressive stress parallel to the belt during a period of decreased compressive stress perpendicular to the belt (Molnar & Lyon-Caen 1988, Mancktelow 1992). The tectonic setting of the Veiga Massif corresponds with an extension perpendicular to the local shortening direction (Fig. 12). This shortening direction is at the same time perpendicular to the regional E–W shortening in the Iberian arc (Bard *et al.* 1973). This superimposition of E–W and N–S shortening directions at the regional scale also occurred in the external zones of the Iberian arc during the Carboniferous (Alvarez-Marrón & Pérez-Estaún 1988, Farias & Marquínez 1991).

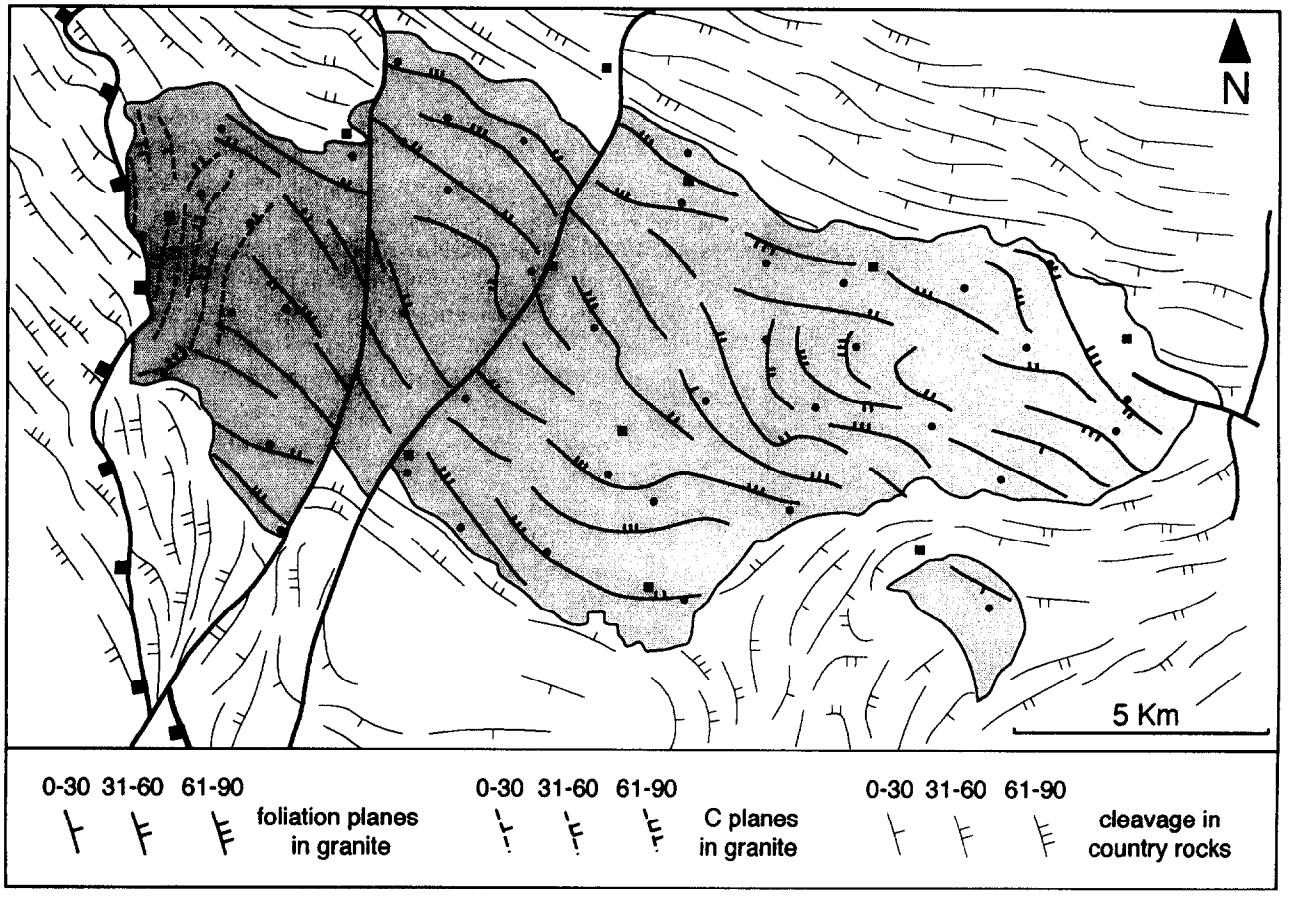

a

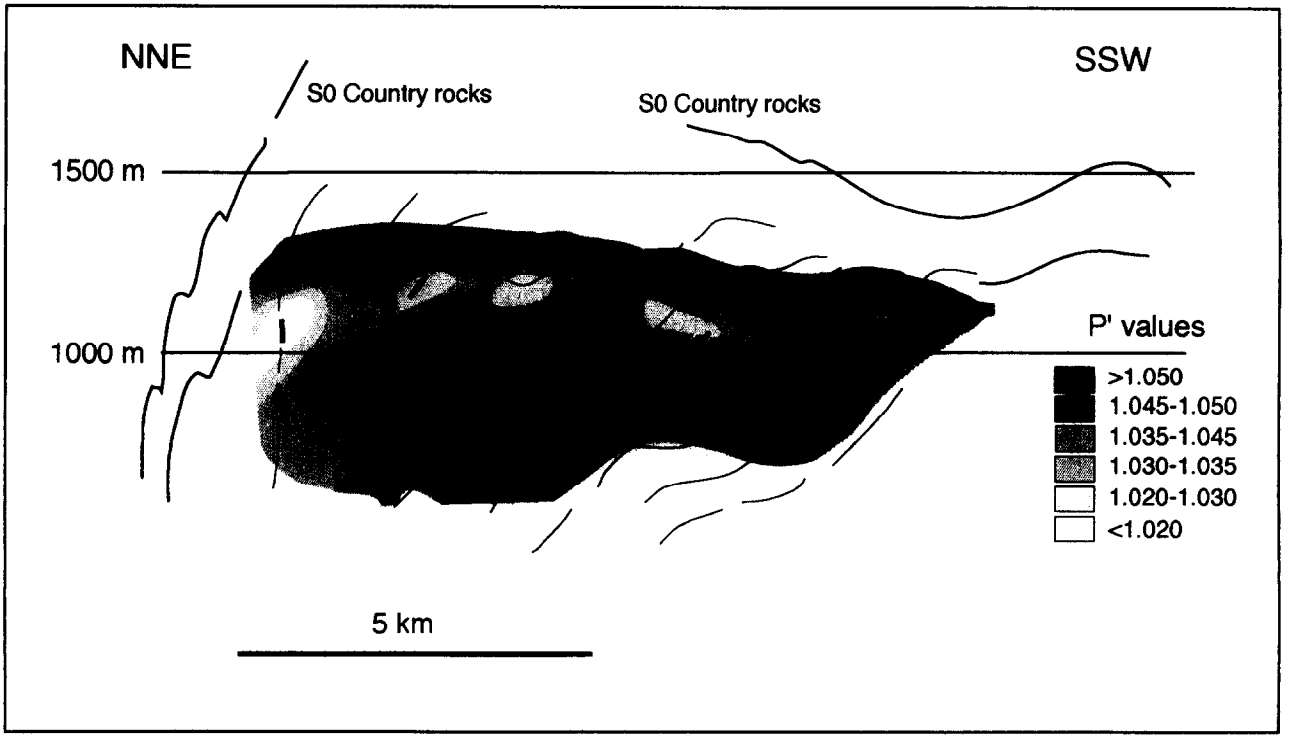

b

Fig. 10. (a) Interpreted trajectories of planes of magmatic foliation and *C* planes obtained from the structural and magnetic analysis. (b) Projection of foliation planes onto a vertical plane perpendicular to the WNW–ESE elongation axis of the Veiga Massif. Contours show the anisotropy index *P'* of the magnetic ellipsoids.

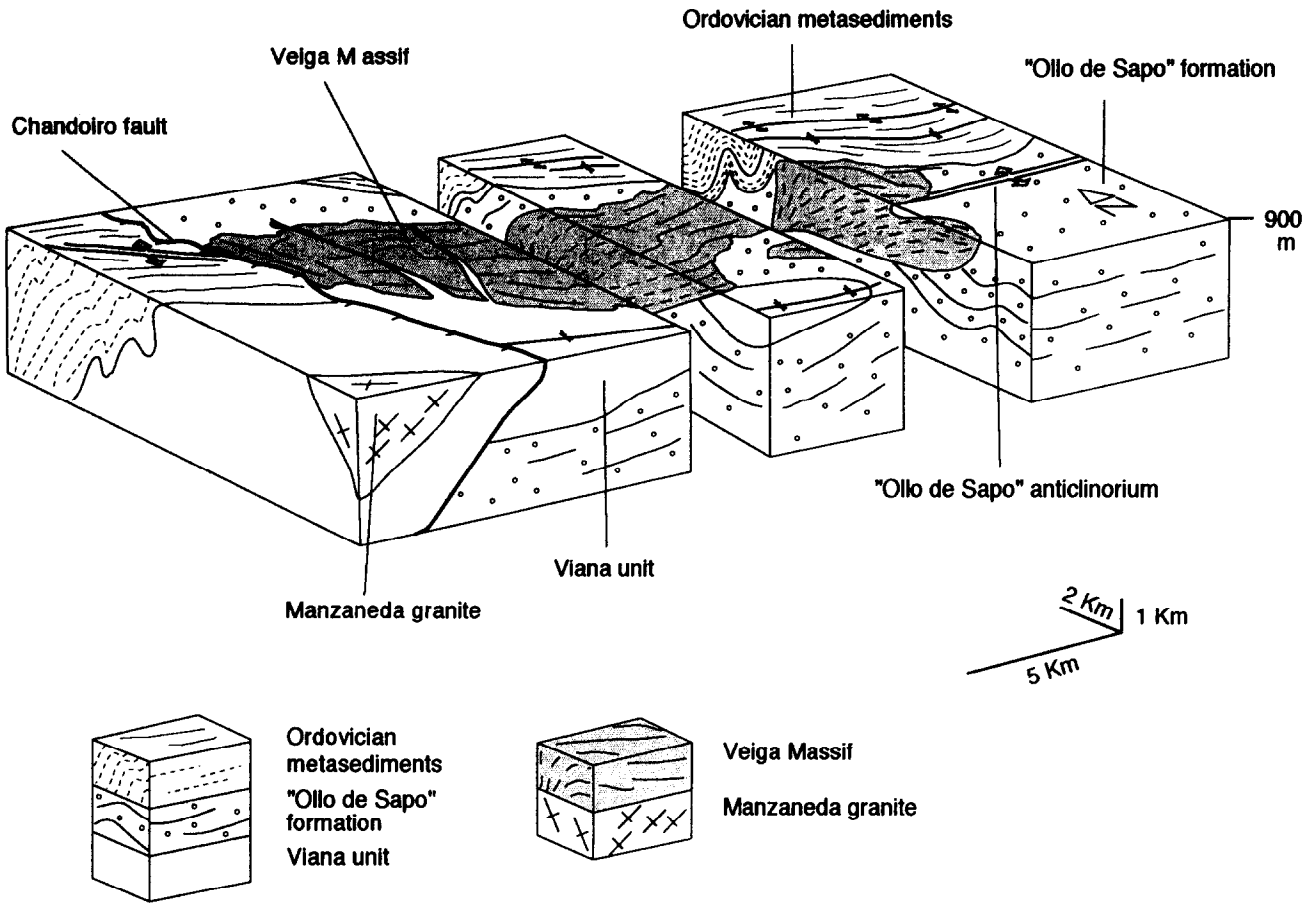

Fig. 11. Schematic block diagram showing the interpreted geometry of the Veiga Massif and its relationship with the structures of the country rock. The displacement produced by the two large N–S to NNE–SSW Late Variscan faults has been restored in order to reconstruct the initial shape of the pluton.

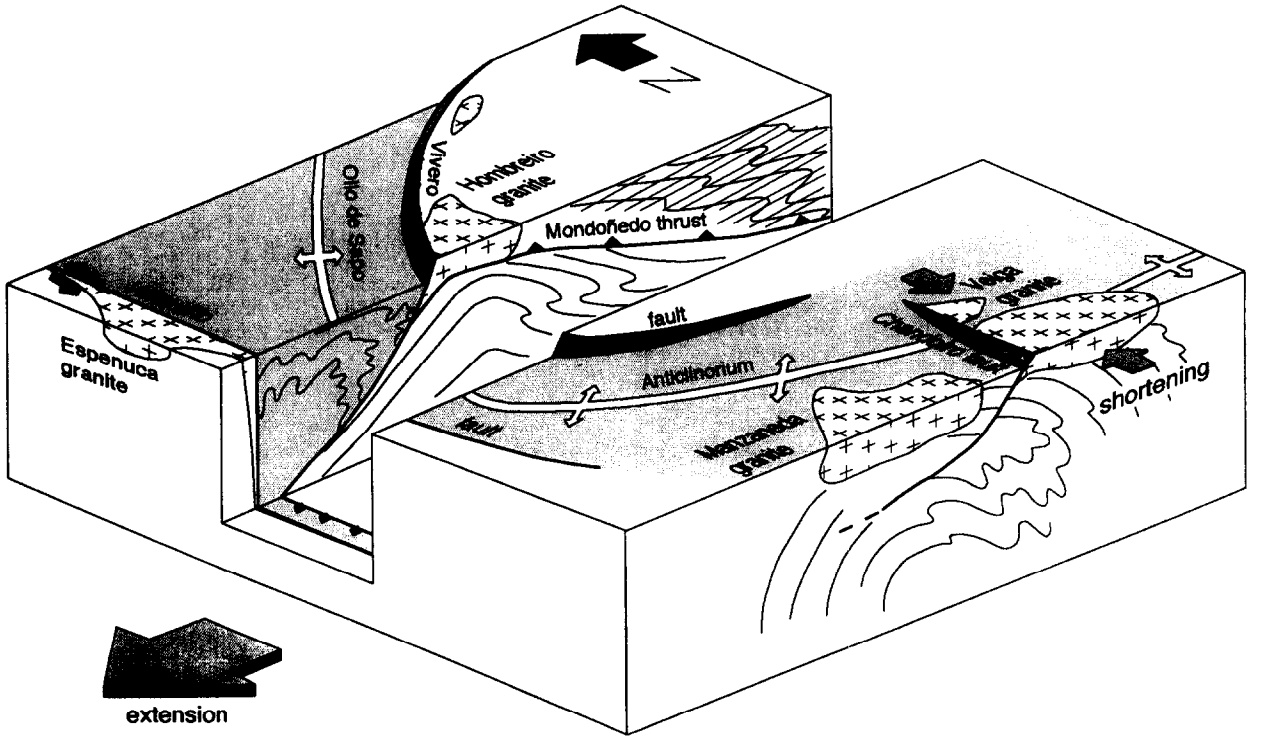

Fig. 12. Schematic block diagram, at the scale of the Hercynian Arc of Galicia, showing the relationship of the Chandoiro fault with the Vivero fault and other granitoid bodies (for a true scale and location, see Fig. 1).

The extension direction indicated by the Chandoiro fault is similar to the extension direction of the Vivero fault, the main extensional structure in the northern part of the Iberian Massif (Martínez-Catalán 1985, Aranguren *et al.* 1990, Aranguren & Tubía 1992), also dipping westward (Fig. 12). As the Chandoiro fault, the Vivero fault cuts across the 'Ollo de Sapo' anticlinorium and is related to the emplacement of granitoids, showing *C–S* structures with normal top-to-the-west shear (Aranguren & Tubía 1992, Román-Berdiel 1994) in its footwall (Fig. 12). The structures associated with the emplacement of the Veiga granodiorite provide, therefore, the basis for the relative timing and spatial location of the massif within the context of the Iberian arc.

CONCLUSIONS

1. Measurement of feldspar orientations and AMS throughout the Veiga granodiorite are consistent and indicate a foliation striking WNW–ESE (parallel to late regional folding), with a constant dip of 75–85°N.

2. A zonation of the igneous body from the southern and western borders (more basic) to the central part and northeastern border (more acidic) is deduced from the bulk low-field susceptibility.

3. The highest degree of magnetic anisotropy is observed in areas located near the bottom and top of the intrusion.

4. Foliation is convergent toward the bottom of the intrusion, along a line located at its northern border, where the magma source is interpreted to be located.

5. The western border of the Massif is affected by *C–S* structures which indicate that the cooling of magma was coeval with movement of the Chandoiro normal fault.

In summary, our structural, magnetic and petrofabric data clearly show that intrusion of the Veiga granodiorite was coeval with NNE–SSW shortening, defined by the D_3-deformation regional phase, and that the cooling of the Massif was coeval with the N290E extensional motion of the Chandoiro Fault.

Acknowledgements—We thank D. Gapais for his critical revision, involving stimulating ideas as well as corrections; J. M. Parés, M. Garcés, A. G. Imaz and E. Arranz for their help with AMS and thin-section analysis and interpretation; J. L. Boucher, J. M. Tubía and C. W. Passchier for their detailed reviews; I. Gil-Peña, C. Maldonado-Bravo and A. Herranz for their help with collection of samples. This work was supported by the Spanish Ministry of Education and Science (research grant to TRB).

REFERENCES

Aranguren, A. & Tubía, J. M. 1992. Structural evidence for the relationship between thrusts, extensional faults and granite intrusions in the Variscan belt of Galicia (Spain). *J. Struct. Geol.* **14**, 1229–1237.

Aranguren, A. & Tubía, J. M. 1994. Características estructurales y modelo de empazamiento del plutón de Guitiriz (Galicia). *Rev. Soc. Esp. Geol.* **7(1–2)**, 63–73.

Arthaud, F. & Matte, P. 1977. Late Paleozoic strike-slip faulting in southern Europa and northern Africa: result of a right-lateral shear zone between the Appalachians and the Urals. *Geol. Soc. Am. Bull.* **88**, 1305–1320.

Bard, J. P., Capdevila, R., Matte, P. & Ribeiro, A. 1972. Le Précambrien de la Meseta Ibérique. *Not. Serv. Geol. Marruecos* **236**, 315–335.

Bard, J. P., Capdevila, R., Matte, P. & Ribeiro, A. 1973. Geotectonic model for the Iberian Variscan orogen. *Nature Phys. Sci.* **241**, 50–52.

Barrera-Morate, J. L., Farias-Arquer, P., González-Lodeiro, F., Marquínez-García, J., Martín-Parra, L. M., Martínez-Catalán, J. R., Del-Olmo-Sanz, A. & Pablo-Marciá, J. G. 1989. Memoria y hoja n°17.27 (Ourense/Verín). *Mapa Geol. Esp.* E. 1:200.000 ITGE, Madrid.

Bastida, F., Aller, J. & Fernandez-Viejo, G. 1993. The structure of the Ollo de Sapo antiform in the Cantabrian coast (NW Spain). *Rev. Soc. Esp. Geol.* **6**(3–4), 93–103.

Bastida, F., Martínez-Catalán, J. R. & Pulgar, J. A. 1986. Structural, metamorphic and magmatic history of the Mondoñedo Nappe (Hercynian belt, NW Spain). *J. Struct. Geol.* **8**, 415–30.

Bateman, R. 1984. On the role of diapirism in the segregation, ascent and final emplacement of granitoid magmas. *Tectonophysics* **110**, 211–231.

Berthé, D., Choukroune, P. & Jégouzo, P. 1979. Orthogneiss, mylonite and non coaxial deformation of granites: the example of the South Armorican shear zone. *J. Struct. Geol.* **1**, 31–42.

Bingham, C. 1974. An antipodally symmetric distribution on the sphere. *Ann. Statist.* **2**, 1201–1225.

Bouchez, J. L. & Pêcher, A. 1981. The Himalayan main central thrust pile and its quartz-rich tectonites in central Nepal. *Tectonophysics* **78**, 23–50.

Brun, J. P., Gapais, D., Cogné, J. P., Ledru, P. & Vigneresse, J. L. 1990. The Flamanville granite (northwest France): an unequivocal example of a syntectonically expanding pluton. *Geol. J.* **25**, 271–286.

Brun, J. P. & Pons, J. 1981. Strain patterns of pluton emplacement in a crust undergoing non-coaxial deformation, Sierra Morena, Southern Spain. *J. Struct. Geol.* **3**, 219–229.

Capdevila, R. & Floor, P. 1970. Les différents types de granites hercyniens et leur distribution dans le Nord Ouest de l'Espagne. *Bol. Geol. Min.* **LXXXI**, 215–225.

Castro, A. 1986. Structural pattern and ascent model in the Central Extremadura batholith, Hercynian belt, Spain. *J. Struct. Geol.* **8**, 633–645.

Castro, A. 1987. On granitoid emplacement and related structures. A review. *Geol. Rundsch.* **76**, 101–124.

Corretgé, L. G., Fernandez, J., Rodríguez, L. & Suárez, O. 1989. Aspectos estructurales del plutón tonalítico de Zarza la Mayor-Ceclavín (NO Cáceres, España). *Stud. Geol. Salmanticensia* **4**, 171–187.

Courrioux, G. 1983. Exemple de mise en place d'un leucogranite pendant le fonctionnement d'une zone de cisaillement: le granite hercynien de Puentedeume (Galice, Espagne). *Bull. Soc. géol. Fr.* **7**, XXV, 301–307.

Courrioux, G., Gagny, C. & Gouanvic, Y. 1986. Analyse de structures cisaillantes dans des granites syntectoniques de Galice (NW Espagne). *Bol. Geol. Min.* **XCVII–VI**, 737–756.

Ellwood, B. B. & Wenner, D. B. 1981. Correlation of magnetic susceptibility with $_{18}O/_{16}O$ data in late orogenic granites of the southern Appalacian Piedmont. *Earth Planet. Sci. Lett.* **54**, 200–202.

Farias, P. 1990. *La geología de la región del sinforme de Verín (Cordillera Herciniana, NW de España)*. Lab. Xeol. Laxe, Nova Terra 2, O Castro, A Coruña, p. 201.

Ferragne, A. 1972. Le Précambrien et le Paléozoique de la Province d'Orense (nord-ouest de l'Espagne). Thèse, Université de Bordeaux 1, 249.

Fisher, R. A. 1953. Dispersion on a sphere. *Proc. R. Soc. Lond.* **A217**, 295–305.

Flinn, D. 1978. Construction and computation of three-dimensional progressive deformations. *J. geol. Soc. Lond.* **135**, 291–306.

Gapais, D. & Barbarin, B. 1986. Quartz fabric transition in a cooling syntectonic granite (Hermitage Massif, France). *Tectonophysics* **125**, 357–370.

Gapais, D. & Cobbold, P. R. 1987. Slip system domains. 2. Kinematic aspects of fabric development in polycrystalline aggregates. *Tectonophysics* **138**, 289–309.

Gapais, D. & White, S. H. 1982. Ductile shear bands in a naturally deformed quartzite. *Textures Microstruct.* **5**, 1–17.

Gleizes, G., Nédélec, A., Bouchez, J.-L., Autran, A. & Rochette, P. 1993. Magnetic susceptibility of the Mont Louis–Andorra ilmenite-type granite (Pyrenees): a new tool for the petrographic characteriz-

ation and regional mapping of zoned granite plutons. *J. geophys. Res.* **98**, 4317–4331.
Gonzalez-Lodeiro, F. & Iglesias, M. 1977. Memoria y Hoja N° 156 (Monforte de Lemos). *Mapa Geol. Esp.* E. 1:50000. IGME, Madrid.
Guillet, P., Bouchez, J. L. & Wagner, J. J. 1983. Anisotropy of magnetic susceptibility and magnetic structures in the Guérande Massif (France). *Tectonics* **2**, 419–429.
Heller, F. 1973. Magnetic anisotropy of granitic rocks of the Bergell Massif (Switzerland). *Earth Planet. Sci. Lett.* **20**, 180–188.
Hrouda, F. 1982. Magnetic anisotropy of rocks and its application in geology and geophysics. *Geophys. Surveys* **5**, 37–82.
Hutton, D. H. W. 1988. Granite emplacement mechanisms and tectonic controls: inferences from deformation studies. *Trans. R. Soc. Edinb. Earth Sci.* **79**, 245–255.
Iglesias, M. & Chouckroune, P. 1980. Shear zones in the Iberian Arc. *J. Struct. Geol.* **2**, 63–68.
Iglesias, M. & Varea, R. 1982. Memoria y Hoja N° 288 (Viana del Bollo). *Mapa Geol. Esp.* E. 1:50000. IGME, Madrid.
Irving, E., Molyneux, L. & Runcorn, S. K. 1966. The analysis of remanent intensities and susceptibilities of rocks. *Geophys. J. R. astr. Soc.* **10**, 451–464.
Jelinek, V. 1977. The statistical theory of measuring anisotropy of magnetic susceptibility of rocks and its application. *Brno. Geofyzika*, pp. 1–88.
Jelinek, V. 1978. Statistical processing of magnetic susceptibility measured in groups of specimens. *Stud. Geophys. Geod.* **22**, 50–62.
Jelinek, V. 1981. Characterization of the magnetic fabric of rocks. *Tectonophysics* **79**, 63–70.
Julivert, M., Marcos, A. & Truyols, J. 1972. L'évolution paléogéographique du NW de l'Espagne pendant l'Ordovicien–Silurien. *Bull. Soc. Géol. Min. Bretagne* **C**, IV, 1–7.
Kukowski, N. & Neugebauer, H. J. 1990. On the ascent and emplacement of granitoid magma bodies—dynamic–thermal numerical models. *Geol. Rundsch.* **79**, 227–239.
Lagarde, J. L. 1987. Les plutons granitiques hercyniens marqueurs de la déformation crustale. L'exemple de la méséta marocaine. Thèse d'Etat, Université de Rennes.
Leblanc, D., Gleizes, G., Lespinasse, P., Oliver, P. & Bouchez, J. L. 1994. The Maladeta granite polydiapir, Spanish Pyrenees: a detailed magneto-structural study. *J. Struct. Geol.* **16**, 223–235.
LeCorre, C. & Saquaque, A. 1987. Comportement d'un système pluton-encaissant dans un champ de déformation régionale: le granite du Bramram (Jebilet, Maroc hercynien). *Bull. Soc. geol. Fr.* **4**, 665–673.
Lienert, 1991. APLOT10. *A program for plotting AMS directions and their elliptical error limits*. Hawaii Institute of Geophysics/SOEST. Honolulu.
Lister, G. S. & Williams, P. F. 1979. Fabric development in shear zones: theoretical controls and observed phenomena. *J. Struct. Geol.* **4**, 283–297.
López-Plaza, M. & Gonzalo, J. C. 1986. Los granitos hercínicos como indicadores de la evolución estructural del Macizo Hespérico. *Hercynica* **II**, 57–64.
López-Plaza, M. & Martínez-Catalán, J. R. 1987. Síntesis estructural de los granitoides hercínicos del Macizo Hespérico. In: *Geología de los Granitoides y Rocas asociadas del Macizo Hespérico. Libro Homenaje a L.C. García de Figuerola*. Rueda, Barcelona, pp. 195–210.
Lotze, F. 1945. Einige probleme der Iberischen Meseta. *Geotect Fersch* **6**, 1–12.
Marcos, A. 1971. Cabalgamientos y Estructuras menores asociadas originados en el transcurso de una nueva fase herciniana de deformación en el occidente de Asturias (NW de España). *Brev. Geol. Astúrica* **XV**, 59–64.
Marcos, A. 1973. Las series de Paleozoico Inferior y la estructura herciniana del occidente de Asturias (NW de España). *Trabajos de Geología* **6**, 1–111.
Martínez-García, E. 1969. Nota sobre la posición del Ollo de Sapo en las provincias de Zamora y Orense. *Com. Serv. Geol. Port.* **LIII**, 37–42.
Martínez-García, E. 1971. Esquema geológico del Noroeste de la provincia de Zamora. *I Congr. Hisp.-Luso-Americ. Geol. E. con. Sic. I* **I**, 273–286.
Martínez-García, E. 1973. Deformación y metamorfismo en la zona de Sanabria (Prov. de Zamora, León y Orense, Noroeste de España). *Stud. Geol.* **V**, 7–106.
Martínez-García, E. & Quiroga, J. L. 1993. Structure of the Ollo de Sapo antiform in the Sanabria–Alcañices area (Zamora, Orense, NW Spain). *Cuaderno Lab. Xeol. Laxe* **18**, 27–35.
Martínez-Catalán, J. R. 1985. *Estratigrafía y Estructura del Domo de Lugo (Sector Oeste de la zona Asturoccidental-leonesa)*. Lab. Geol. Lage, Segunda Serie II. A Coruña, p. 291.
Martínez-Catalán, J. R., Gonzalez-Lodeiro, F., Iglesias, M. & Diez-Balda, M. A. 1977. La estructura del Domo de Lugo y del anticlinorio del Ollo de Sapo. *Stud. Geol.* **12**, 109–122.
Matte, P. 1968. La structure de la virgation hercynienne de Galicia (Espagne). *Geol. Alpine* **44**, 1–127.
Miller, C. F., Watson, E. B. & Harrison, T. M. 1988. Perspectives on the source, segregation and transport of granitoid magmas. *Trans. R. Soc. Edinb. Earth Sci.* **79**, 135–156.
Parés. J. M. 1988. La utilización de la anisotropía de la susceptibilidad magnética (ASM) en el estudio de la deformación finita: ejemplo de la zona milonítica de Cap de Creus (Catalunya). *Geogaceta* **5**, 50–53.
Parga-Pondal, I. 1963. Rocas y minerales de interés económico del macizo galaico. *Trabajos del Laboratorio geológico de Lage (la Coruña)* **14**, 99–104.
Paterson, S. R. & Fowler, K. 1993. Re-examining pluton emplacement processes. *J. Struct. Geol.* **15**, 191–206.
Pitcher, W. S. 1979. The nature, ascent and emplacement of granitic magmas. *J. geol. Soc. London* **136**, 627–662.
Ramsay, J. G. 1967. *Folding and Fracturing of rocks*. McGraw-Hill, New York.
Ramsay, J. G. & Graham, R. H. 1970. Strain variation in shear belts. *Can. J. Earth Sci.* **7**, 786–813.
Ribeiro, A. 1970. Position structurale des Massifs de Morais y Bragança (Tras-os-Montes). *Com. Serv. geol. Portugal* **104**, 115–130.
Ribeiro, A. 1974. Contribution à l'étude tectonique de Tras-os-Montes oriental. *Serv. geol. Portugal* **24**.
Roberts, J. L. 1982. *Introduction to Geological Maps and Structures*. Pergamon Press, Oxford, p. 331.
Rochette, P. 1987. Magnetic susceptibility of the rock matrix related to magnetic fabric studies. *J. Struct. Geol.* **9**, 1015–1020.
Román-Berdiel, T. 1994. Mécanismes d'intrusion des granites supracrustaux: modèles analogiques et exemples naturels. Thèse d'Université. Rennes, p. 247.
Simpson, C. 1985. Deformation of granitic rocks across the brittle–ductile transition. *J. Struct. Geol.* **7**, 503–511.
Tarling, D. H. 1966. The magnetic intensity and susceptibility distributions in some Cenozoic and Jurassic basalts. *Geophys. J. R. astr. Soc.* **11**, 423–432.
Tarling, D. H. & Hrouda, F. 1993. *The Magnetic Anisotropy of Rocks*. Chapman & Hall, London, p. 217.
Tommasi, A., Vauchez, A., Fernandes, L. A. D. & Porcher, C. C. 1994. Magma-assisted strain localization in an orogen-parallel transcurrent shear zone of southern Brazil. *Tectonics* **13**, 421–437.
Vauchez, A. 1987. The development of discrete shear zones in a granite: stress, strain and changes in deformation mechanisms. *Tectonophysics* **133**, 137–156.
Wickham, S. M. 1987. The segregation and emplacement of granitic magmas. *J. geol. Soc. London* **144**, 281–297.

APPENDIX
METHODOLOGY FOR THE STUDY OF MAGNETIC PROPERTIES

Statistical treatment and reliability of data of AMS

Two types of distribution for the AMS directional data can be considered:

(1) Fisher's unimodal distribution: for each axis, Fisher (1953)'s probability function calculates the mean direction and its associated error (given by a confidence α_{95} cone, and a precision parameter K). This is the classical method to obtain mean directions for the three axes of the MS tensor. Nevertheless, this method does not give real values when AMS values do not present a unimodal distribution.

(2) Bingham (1974)'s bimodal distribution considers a distribution with two probability maxima and refers them to a second range matrix with three eigenvectors (E_1, E_2 and E_3). We have used this method when the associated error (α_{95}) of Fisher's distribution was greater than 10°. The mean was characterized with the direction and value of the third eigen-vector (the pole to the plane which contains the spatial variability for this axis). This method is especially useful in the case of uniaxial tensors ($K_2 \approx K_3$ or $K_1 \approx K_2$). In this case, the vectors showing the orientation of the two identical axes are contained within a plane and its sum nears one. The plane which contains E_1 and E_2 is the plane whose pole is the third axis of the MS tensor, K_1 (when $K_2 = K_3$) or K_3

(when $K_1 = K_2$). In our opinion (see also Tarling & Hrouda 1993), it is better to use an orthogonal two-pole distribution referring it with E_1 and E_3 (considering both orientation and value) of the Bingham distribution (see Table 1).

There exists another useful method based on Jelinek (1978)'s statistical theory of AMS data, based on averaging all susceptibility tensors after they have been normalized against their main susceptibility. The variance and confidence intervals for the orientations of the principal susceptibilities are computed from the variance-covariance matrix. In that case, the confidence area about each mean principal direction is elliptical, so that the maximum and minimum radii are required to define this area on a representative sphere (Tarling & Hrouda 1993). We used an approximation of this method with the help of a special software package (Aplot10 program, Lienert 1991) in order to contrast the graphical error estimation of this method with the two methods above described.

We have used the arithmetic mean of the Km together with the absolute error value (see Table 1). The relative errors obtained are less than 10% and 15% for 61% and 88% of the specimens, respectively.

For the treatment of errors associated to mean values of parameters P' and T, log-normal distributions have been considered. For P', 88% of sites show errors lower than 15% and 64% of sites lower than 10%. The reason for low errors is that P' is proportional to the principal K_1–K_3 section of the ellipsoid.

In order to evaluate the spatial distribution of the values of the different parameters (P', T) and variables (Km) we have considered these as a linear and continuous functions and made a spatial interpolation in two dimensions, drawing maps which show this variability.